Nontrivial strength of van der Waals epitaxial interaction in soft perovskites

Yiping Wang,[1] Lei Gao,[2,*] Yunbo Yang,[3,†] Yu Xiang,[3] Zhizhong Chen,[1] Yongqi Dong,[4] Hua Zhou,[4] Zhonghou Cai,[4] Gwo-Ching Wang,[3] and Jian Shi[1,‡]

[1]*Department of Materials Science and Engineering, Rensselaer Polytechnic Institute, Troy, New York 12180, USA*

[2]*Corrosion and Protection Center, Key Laboratory for Environmental Fracture (MOE), University of Science and Technology Beijing, Beijing 100083, China*

[3]*Department of Physics, Applied Physics, and Astronomy Rensselaer Polytechnic Institute, Troy, New York 12180, USA*

[4]*X-ray Science Division, Argonne National Laboratory, Lemont, Illinois 60439, USA*

(Received 24 February 2018; published 27 July 2018)

The van der Waals (vdW) bond is traditionally believed to be orders of magnitude lower than the typical chemical bond (i.e., ionic, metallic, or covalent), and hence the effects caused by a vdW interface are thought to be trivial. In this paper, by investigating the vdW epitaxial growth of a mechanically soft perovskite on the vdW substrate, we obtained the solid proof of strong non-negligible vdW interaction. The experimental results illustrate the formation of cracks and holes for the relaxation of the vdW strain as well as a lattice-constant-dependent epitaxial angle evolution and a pronounced band-structure change. The first-principles calculations indicate that the contribution of the vdW interaction energy at the epitaxial interface reaches up to more than a quarter of the overall interaction energy far exceeding the traditionally recognized vdW bonding strength. Both the experimental and the theoretical work show that given the appropriate material system, the vdW interaction could be strong enough to significantly manipulate material properties.

DOI: 10.1103/PhysRevMaterials.2.076002

The van der Waals (vdW) interaction is a dipole-dipole force [1] that is traditionally considered much weaker than a chemical bond which involves a permanent charge-transfer/sharing process. Consequently, the vdW bonding strength is normally thought of as trivial and can be easily disturbed or altered. By taking advantage of that, mechanical exfoliation was first applied to obtain the atomically thin two-dimensional graphene from graphite [2,3] together with a whole family of two-dimensional materials including hexagonal boron nitride (h-BN) [4], transition-metal dichalcogenides [5,6], etc. As a step forward, heteroepitaxy is found to exist between two different vdW bonded materials and hence comes the vdW epitaxial growth [7,8]. Different from the traditional chemical epitaxy, vdW epitaxy lifts the restriction of rigid lattice match and even lattice symmetry thanks to the weaker interfacial interaction [7,9,10]. VdW epitaxially grown thin films are usually believed to be in a freestanding nature with few defects that can lead to a high mobility and good properties [10,11]. Over the years, various materials have been proven to grow epitaxially on a single mica substrate by vdW epitaxy [8], which includes both naturally layered materials (transition-metal dichalcogenides, metal halides, etc.) and nonlayered materials (halide perovskite, metal oxides, group II–VI materials, etc.). Like a double edge sword however, vdW epitaxy largely broadens the material selection but at the same time is generally believed to be unable to manipulate the overlayer property via the substrate effect. However, if indeed strain engineering also exists in the vdW epitaxy, one of the major benefits would then be the capability to strain materials that are hard to obtain via conventional epitaxy, i.e., materials whose suitable substrates are yet to be found.

Despite the above commonly accepted understandings of vdW interaction, there are more and more observations that indicate otherwise as the research on two-dimensional materials deepens. For example, ultraflat graphene is and can only be obtained when muscovite mica, a layered substrate, is supported underneath [12]. The experimental observation as well as subsequent theoretical work [13] both indicate a strong interaction that can be vdW in nature. At the same time, a strong interlayer electron-phonon interaction between h-BN and WSe_2 was observed [14], indicating a nontrivial vdW interface. For the epitaxial vdW heterostructure, largely strained growth of an organic thin film on a mica substrate has been demonstrated [15]. Recently for the pure inorganic material system, an incommensurate-commensurate transition was observed for h-BN and graphene that resulted in a large vdW strain [16]. Previously we have also studied the possible vdW strain engineering on PbI_2 [17]. Even for a quasi-vdW epitaxial growth, e.g., only one of the films/substrates is a layered material, it is found that the choice of substrate can result in a significant strain of a presumably strain-free two-dimensional material [18].

With the discrepancy between the assumptions and the observation in the vdW interaction, there are, of course, intriguing questions remains to be answered. Since the interlayer vdW interaction is so trivial, why can epitaxies always be formed? When a quasi-vdW epitaxy is formed, what is the nature of the interface interaction? Is there a case when vdW interaction could be strong enough so that the conventional strain

*gaolei@ustb.edu.cn

†Present address: Hermes Microvision Inc., San Jose, California, 95131.

‡Corresponding author: shij4@rpi.edu

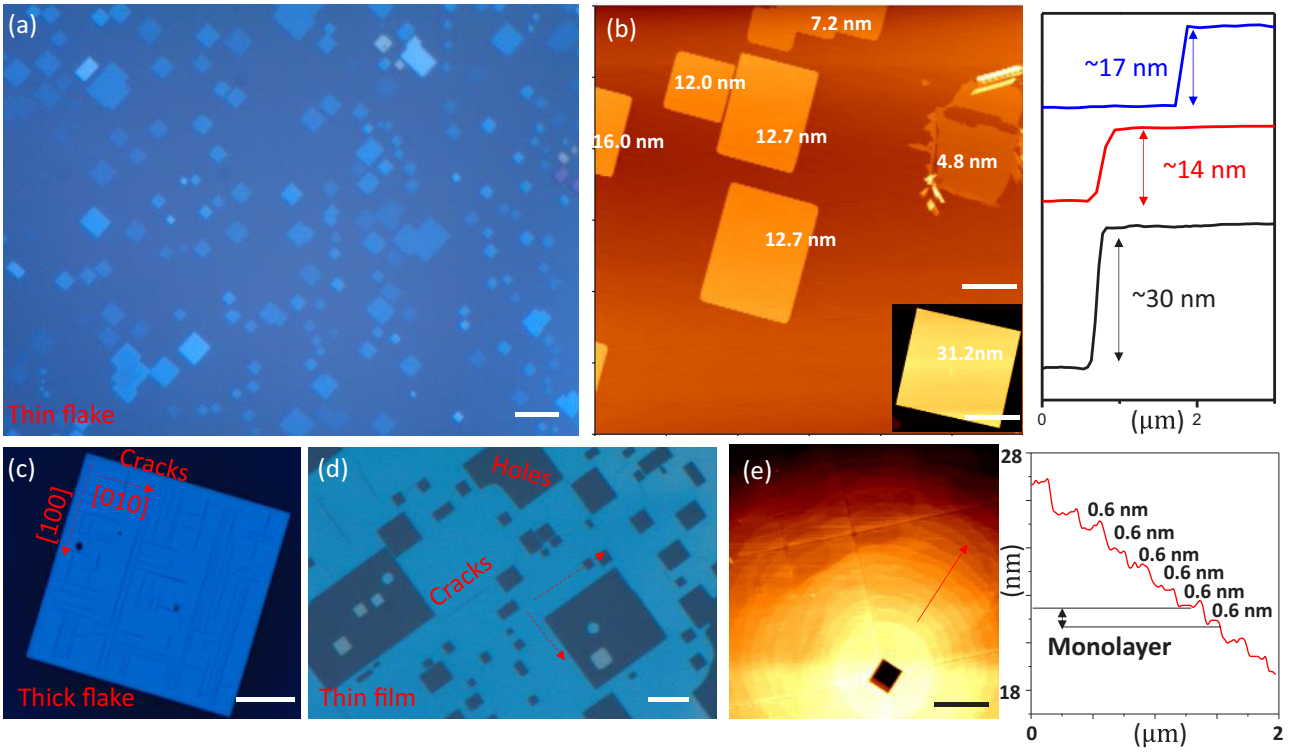

FIG. 1. Morphology characterization of halide perovskite flakes grown on a mica substrate. (a) Optical image of large-scale growth of epitaxial $MAPbBr_3$ on a mica substrate. The square flakes of halide perovskite are aligned into one direction, and the similar color reflects a small thickness variation. (b) AFM characterization of the flakes in (a), and the individual flake thickness is labeled. The inset shows another thicker flake also with a very smooth surface. The right of (b) shows the thickness profiles of three individual halide perovskite flakes. (c) Optical image of a large thick $CsPbBr_3$ square flake with perpendicular cracks on the surface. The crystallographic orientations of the crack have been labeled. (d) Optical image of a $CsPbBr_3$ thin film with square holes and cracks on the surface. The cracks and holes can be viewed as signs of strain relaxation. (e) AFM characterization of the holes in a $MAPbBr_3$ thin film on mica. At the vicinity of the square hole there exist terraces of monolayer thickness (shown by the height profile on the right). Perpendicular lines with 45° to the edge of the square can also be observed, which are hypothesized to be [110] dislocations. [Scale bar: (a) 10 μm; (b) 5 μm; (c) 30 μm; (d) 10 μm; (e) 1 μm.]

engineering occurring in chemical epitaxy can be repeated? Can the vdW interaction be more pronounced if the growth material is mechanically soft in nature and at the same time contains heavy elements since the vdW interaction scales with atomic weight? In this paper, we attempt to address these questions by studying the vdW epitaxial growth of $CH_3NH_3(MA)/CsPbX_3$ (where MA represents methylammonium and X represents Cl, Br, and I), an emerging semiconducting material family with the Young's modulus ranging from 14 to 19 GPa [19–21] on the mica substrate. From our previous experience with halide perovskite [9,22], single-crystalline and epitaxial flakes were grown. Thanks to the soft nature of the halide perovskite material [23], we found solid evidence both from morphology and structural and optical characterizations that indicate a very strong non-negligible vdW interaction existing between mica and halide perovskite and the possible existence of significant vdW strain. By performing the density functional theory (DFT) calculations, we studied the nature of bonding at the halide perovskite/mica interface and revealed the indispensable role of vdW interaction. Our paper shows that by the proper selection of the material systems, the strength of vdW epitaxial interaction can be fully unleashed to achieve the promising vdW epitaxy-based strain engineering.

Epitaxial halide perovskite has been grown on a mica substrate via chemical vapor deposition with controlled parameters that can influence the flake size and thickness. Additional information concerning the details of the growth setup can be found in the materials growth and characterization in the Supplemental Material [24]. Figure. 1(a) shows an optical image of the large-scale epitaxial growth of $MAPbBr_3$ flakes about ~10 μm in lateral size on the mica substrate. It can be easily observed that all the flakes show a square/rectangular morphology that corresponds to the Wulff construction of the {100} lowest surface energy facets. Meanwhile, the flakes are well aligned towards one single direction that indicates a well-constructed epitaxial relation with the substrate. Moreover, the as-grown flakes show a similar weak color contrast under an optical microscope, indicating a uniform and relatively small thickness. A closer examination of the morphology and thickness profile of the same flakes was performed with an atomic force microscope (AFM) with the resultant image shown in Fig. 1(b). The AFM images show that the halide perovskite has a smooth surface across the whole flake that is comparable to the atomically flat mica surface. The thicknesses of the individual flakes ranging from 4.8 to 16 nm have been labeled. A similar AFM image with a larger scale that contains

more flakes can be found in Fig. S1 of the Supplemental Material [24]. The thinnest flake we have been able to grow so far is about six atomic layers of $MAPbBr_3$. The inset of Fig. 1(b) shows a relatively thicker flake (∼31 nm), nonetheless it has the same surface smoothness. A more clearly quantitative illustration of the thickness profile of three individual flakes is shown to the right of Fig. 1(b) with the surface of each flake showing no observable thickness variation.

However, as the flake grows in both lateral size and thickness, a completely different situation was observed as will be discussed later in Figs. 1(c)–1(e). Figure 1(c) shows a large $CsPbBr_3$ flake with its lateral size exceeding 100 μm and thickness over 100 nm. Surprisingly, well-aligned crack networks parallel to the edges along the ⟨100⟩ directions can be easily observed even with the optical microscope. As a step forward, we found for the even larger area $CsPbBr_3$ thin film not only cracks, but also square holes as displayed in Fig. 1(d). It can be easily seen that for the square holes in Fig. 1(d), still the ⟨100⟩ edge dominates. That the appearance of cracks and holes in thicker and larger flakes and the absence of those in thinner ones, even though both are epitaxial in growth, is of great interest. Holes and cracks are commonly interpreted as signatures of strain relaxation once the film thickness exceeds a critical limit in the conventional chemical epitaxial growth of a thin film [25,26]. The appearance of those, especially in thicker flakes, indicates that, for vdW epitaxy, the interaction at the flake interface is comparably strong and, more importantly, the thinner crack and hole-free flakes may be highly strained due to the soft nature of halide perovskite. To investigate the nature of the morphology of the holes, AFM characterization was further conducted and shown in Fig. 1(e). Consistent with the observation made in optical images, the AFM shows holes on single flakes with sharp ⟨100⟩ edges. Moreover, we also observe at the vicinity of the square hole very clear layer-by-layer terraces with the step height equal to one atomic layer of $MAPbBr_3$ as shown by the height profile to the right of Fig. 1(e). A magnified view of the layer-by-layer terrace can be found in Fig. S2 of the Supplemental Material [24]. The presence of terraces, i.e., the Stranski-Krastanow (SK) growth, is also another typical sign of strain relaxation, although less drastic, compared to the formation of cracks and holes [27,28]. In addition to that, we also observed trench networks 45° to the hole edges (i.e., along the ⟨100⟩ directions). The trenches could be another sign of the SK growth mode and the formation of islands to accommodate strain. More AFM images concerning the relative orientation of the hole edges and the 45° steps can be found in Fig. S3 of the Supplemental Material [24].

Although the morphologies of the as-grown vdW epitaxial halide perovskite flakes show solid evidence of strong interface interaction, the resultant strain and strain relaxation are likely to render a structural reconstruction of halide perovskite compared with the bulk crystal. To investigate the structural information of the epitaxial growth, both synchrotron x-ray diffraction (XRD) and transmission electron microscope (TEM) studies were carried out. Figures 2(a) and 2(b) show the result of synchrotron XRD characterization of the $MAPbBr_3$ flake on a mica substrate under a reflection mode (i.e., the out-of-plane lattice spacing is measured). Taking advantage of

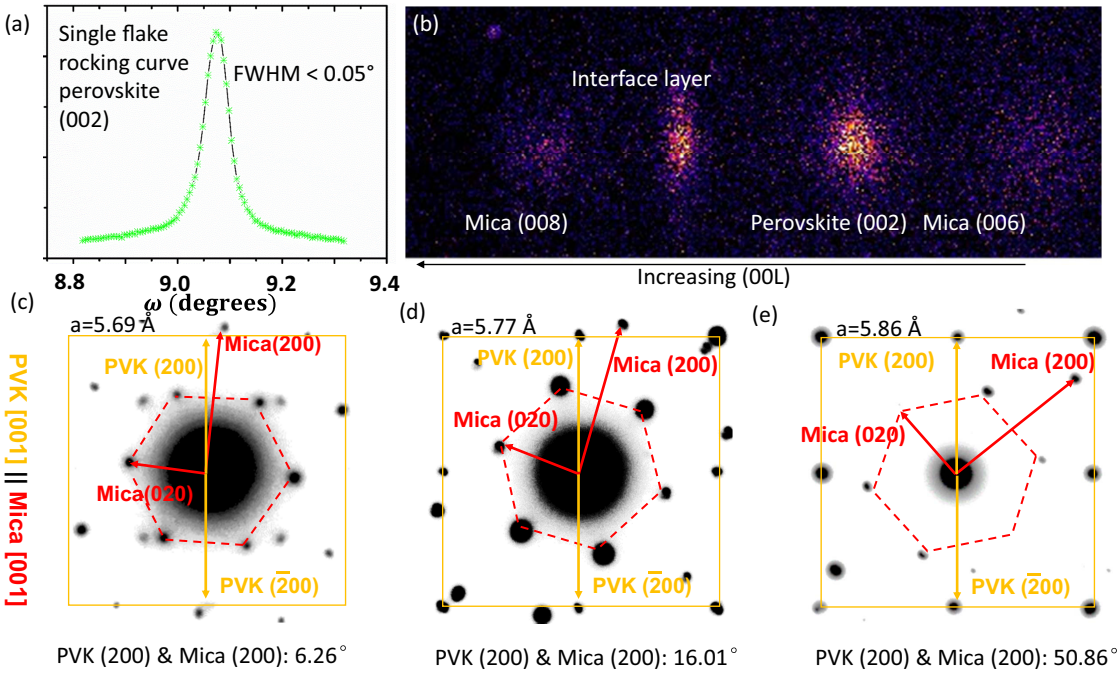

FIG. 2. Structural characterization of an epitaxial halide perovskite on mica. (a) Synchrotron x-ray-diffraction rocking curve of the (002) peak from a single $MAPbBr_3$ flake. (b) Synchrotron x-ray-diffraction 00L scan of halide perovskite on mica. Apart from the (006) and (008) diffractions from mica and the (002) diffraction from perovskite, another diffraction pattern is also recorded that could come from an interfacial layer. (c)–(e) TEM planar view electron diffraction patterns of halide perovskite grown on a mica substrate with (c) $MAPbCl_3$ and (d) and (e) $CsPbBr_3$. Two sets of diffraction spots belonging to the substrate (red) and film (orange) have been indexed. Halide perovskites with different lattice constants result in a different incommensurate epitaxial angle with the mica substrate. The angle dependence of the lattice constant has been labeled.

the nanobeam, we were able to focus the synchrotron x-ray flux into an ∼500-nm spot so that the diffraction information of a single flake can be acquired. Unfortunately, due to the extensive beam damage, only relatively thick flakes can be characterized. Figure 2(a) shows the rocking curve of $MAPbBr_3$ (002) with a full width at half maximum (FWHM) less than 0.05°. This again confirms the high quality single crystallinity of the as-grown flakes. Figure 2(b) shows the θ-2θ out-of-plane scan with the (006) and (008) reflections of the mica substrate and the (002) reflection of $MAPbBr_3$ clearly presented. Interestingly in addition to those, one extra reflection [which is labeled as the "interface layer" in Fig. 2(b)] is also observed that can be fit to neither the flake nor the substrate. The extra spot is very unstable and would disappear soon after a prolonged synchrotron irradiation. With all available knowledge, we hypothesize that the reflection comes from either an interfacial layer that helps better buffering the $MAPbBr_3$ on the mica substrate, or more surprisingly, from a highly strained layer of the perovskite at the interface that rapidly relaxes after an external perturbation (e.g., high-energy synchrotron irradiation). Meanwhile, when the (002) reflection was checked for individual flakes, we still observe a noticeable peak shift with the thinner one being smaller in the out-of-plane spacing (Fig. S4 of the Supplemental Material [24]), indicating possibly some residual compressive out-of-plane strain. Even though we have been unable to characterize the sub-10-nm flakes, by studying the thicker flakes, we are still able to conclude that the flakes are no longer freestanding and strain free as previously assumed.

To better understand the structural information of the film's in-plane orientation with the substrate, we carried out an in-plane TEM electron diffraction analysis of $MAPbCl_3$ and $CsPbBr_3$ flakes on mica. The $CsPbBr_3$ and $MAPbCl_3$ flakes are chosen due to the feasibility of the TEM sample preparation, and at the same time we can see how the epitaxial relationship would be modified if halide perovskites with different lattice constants are grown. In general, the samples tested have lateral dimensions of about micrometers according to the TEM real-space image. The thickness cannot be directly measured by the TEM but estimated being <20 nm based on the growth condition. The resultant TEM diffraction patterns of different crystals are shown in Figs. 2(c)–2(e) where Fig. 2(c) is for $MAPbCl_3$ and Figs. 2(d) and 2(e) are for $CsPbBr_3$ flakes. All the indices of mica have been accurately labeled based on its monoclinic crystal structure. With the limited in-plane TEM samples we can prepare, surprisingly we found that for $CsPbBr_3$ samples, different flakes indeed show different in-plane lattice constants of 5.77 Å in Fig. 2(d) and 5.86 Å in Fig. 2(e), supporting the argument of epitaxial strain for thinner flakes. More interestingly, we also found that as the lattice constants for different halide perovskites change, their epitaxial relationships with the mica substrate also change in a regular pattern. That is, the reciprocal vector offset angle between the perovskite (200) and the mica (200) increased from 6.26° to 50.86° as the lattice constant increases from 5.69 to 5.86 Å. This progressive angle change is in great resemblance to the Novaco-McTague theory [29] where they proposed that when incommensurate epitaxy is formed on a vdW substrate, the incommensurate angle [in our case the angle between perovskite (200) and mica (110)] would gradually change as the lattice constant of the overlayer changes. The angle change itself is believed to be a pathway for strain relaxation. Later experimental results of noble-gas adsorption on graphite successfully proved the theory [30], but so far such angle-dependent incommensurate epitaxy has yet to be proved in inorganic material systems. Therefore, the angle dependence we found would very likely be the result of vdW strain relaxation, and a sound proof of the strong vdW interaction when epitaxy is formed. We believe the observance of the angle dependence is a result of the mechanically soft nature of the halide perovskite and the high mobility of adatoms on a vdW surface. Such angle dependence is again confirmed when we carried out a transmission mode synchrotron diffraction on a group of small epitaxial $CsPbBr_3$ crystals as shown in the result in Fig. S5 of the Supplemental Material [24]. Figure S5 of the Supplemental Material [24] is a magnified portion of a synchrotron diffraction pattern where the diffraction spot dispersion in the radial direction denotes the lattice spacing variation, and the dispersion in the tangential direction denotes the orientation angle dependence. We can clearly observe that, although the diffraction spots for $CsPbBr_3$ have the same "sharpness" as mica in the radical direction, these spots are much more dispersed along the tangential direction that is consistent with our angle-dependent observation in the TEM characterization. The structural characterizations overall indicate that strain may very likely exist at least at the early stages of the vdW epitaxial growth of halide perovskite, which will later relax either by the formation of cracks/holes or through an incommensurate angle.

Meanwhile, we also believe that, if the strong vdW interaction would influence the morphology and structure of halide perovskite, its electronic band structure and optical properties will be altered as well. For that purpose, we conducted a photoluminescence (PL) study on $MAPbBr_3$ flakes with different thicknesses and showed the resultant spectra in Fig. 3(a). By observing the color contrast in optical images we can easily identify the relative thicknesses of the flakes being investigated. Figure 3(a) shows that with decreasing film thickness, we see a uniform trend of a blueshift of PL peaks of $MAPbBr_3$ from about 2.31 eV for a solution-produced bulk single crystal to 2.44 eV for the thinnest $MAPbBr_3$ flake we have been able to characterize. The insets of Fig. 3(a) are the optical images of the individual samples being tested. The lateral sizes of all the flakes tested in Fig. 3(a) are around micrometers, and their thicknesses are well beyond the range of quantum confinement. We did not observe any PL dependence on the lateral size of the flake. The thickness-dependent PL blueshift for halide perovskite has been observed and studied for some time [31–33] with a conclusive explanation yet to come. However, it should also be noted that our result together with other experimental work [33] on epitaxial growth produce a much more drastic thickness dependency compared with other nonepitaxial work [31,32]. Due to the very recent popularity of halide perovskite, there has been very limited study on the conventional epitaxial growth of the material, and we have been demonstrating earlier the epitaxy growth on the NaCl substrate [34]. However, it is found that it is still very challenging to strain the material by NaCl and study

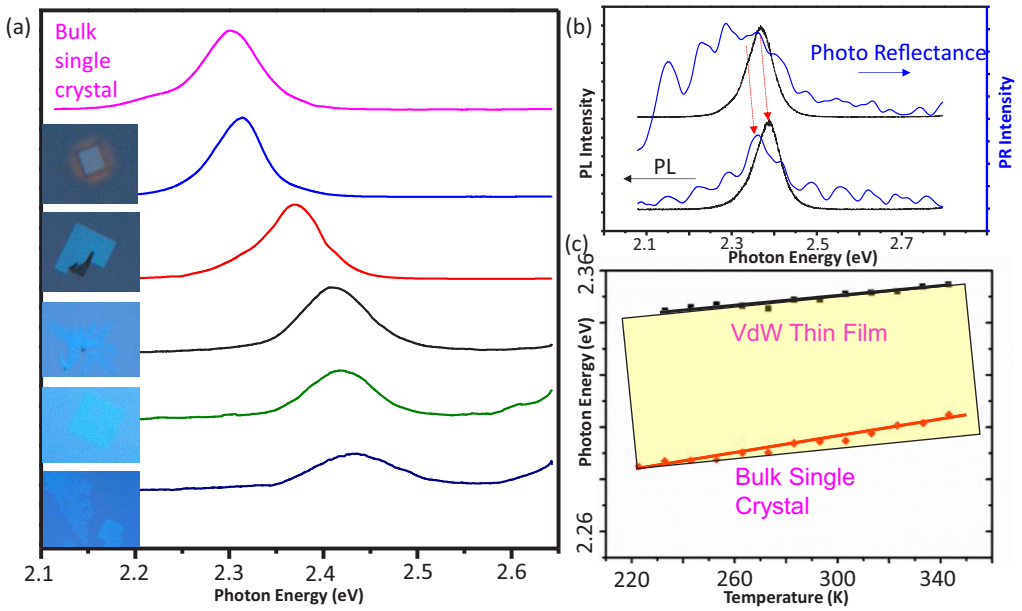

FIG. 3. Optical characterization of halide perovskite flakes on mica. (a) PL spectra of $MAPbBr_3$ flakes with different thicknesses. A significant blueshift of PL peaks with decreasing thickness is observed. The optical image to the left shows each flake where the spectrum is acquired. The color contrast of the optical image can be used to deduce the relative thickness of the flake. (b) PL spectra (black) and micro-PR spectra of the same $CsPbBr_3$ flakes. The two kinds of characterization show a consistent shift of peaks, indicating a difference in the band structure. (c) Temperature-dependent PL spectra of the vdW epitaxial thin film and bulk single crystal. A remarkable difference in the slopes can be observed. The vdW thin film follows more with the thermal expansion of the substrate when changing temperature.

the thickness-dependent PL in that case. The strain will be completely relaxed for thicker films (so there is no PL shift), and for thinner films, Cl will diffuse into the overgrown layer and mediate the lattice mismatch, and the resultant PL will be from the mixed halide perovskite instead of a strained thin-film layer. Nonetheless, the finding in this paper shows a significant thickness-dependent PL shift. Meanwhile we may also exclude other mechanisms that may result in the PL shift. First, for the reabsorption of self-emitted PL [35,36], such a phenomenon can be neglected for thinner flakes and indeed for thicker ones, a shoulder at the low-energy side starts to show up which can be interpreted as the result of self-absorption. Second, we also rule out the Burstein-Moss effect [34] since previously an excitation intensity-dependent PL of similar flakes by us [37] showed no observable peak shift. The intensity-dependent PL can also be referenced to rule out the possibility of an optical Stark effect, a fluence-dependent energy-level splitting phenomenon [38]. To further verify the peak shift comes from a change in the electronic band structure instead of other dynamics, we performed a microphotoreflectance (PR) study on two flakes together with their PL results shown in Fig. 3(b). It can be observed that the peak shift in PR spectra is consistent with the PL difference, indicating that the excitonic effect is negligible, thus the two flakes indeed differ in the band structure since reflectance is an absorption-related first-order effect. With all the discussions above, we have reason to believe that it is the mica substrate and vdW epitaxy that induce a more drastic PL shift. Besides the aforementioned observations, a comparison between the temperature-dependent PL of the vdW flakes and bulk single crystals of $MAPbBr_3$ would give rise to another proof of the strong interaction from the mica substrate. As shown in Fig. 3(c), upon changing temperature, the peak energy from bulk single crystals changed more drastically than that of the vdW flakes. Since for the same kind of material, the electronic band structure is, to a large extent, determined by lattice parameters, the lattice of bulk single-crystal $MAPbBr_3$ changed more drastically compared to the vdW flakes. We tentatively attribute this discrepancy to the interaction with mica substrates. Considering the larger thermal expansion coefficient of halide perovskite [39] than that of mica [40], the thermal expansion of the vdW flakes will be reduced by that from mica, thus a larger thermal strain is observed in bulk single crystals. This observation indicates that the vdW interaction might be strong enough to mediate the mismatched thermal strain during various heating/cooling processes.

All the experimental results above indicate that the bonding nature between a layered mica substrate and a nonlayered halide perovskite is much more intriguing than expected and that the qualitative analysis is insufficient to unveil the fundamental physics. With that consideration, first-principles calculations were carried out to understand the interface between mica and $CsPbBr_3$. The inorganic perovskite is chosen due to its structural simplicity but similar chemical and mechanical properties with its hybrid counterpart. The DFT calculations were carried out with the Vienna *ab initio* simulation package [41]. The projector-augmented-wave method was utilized to model the core electrons [42]. The electron exchange and correlation were modeled within the generalized gradient approximation using the Perdew-Burke-Ernzerhof (PBE) functional [42]. A nonlocal optB86b-vdW

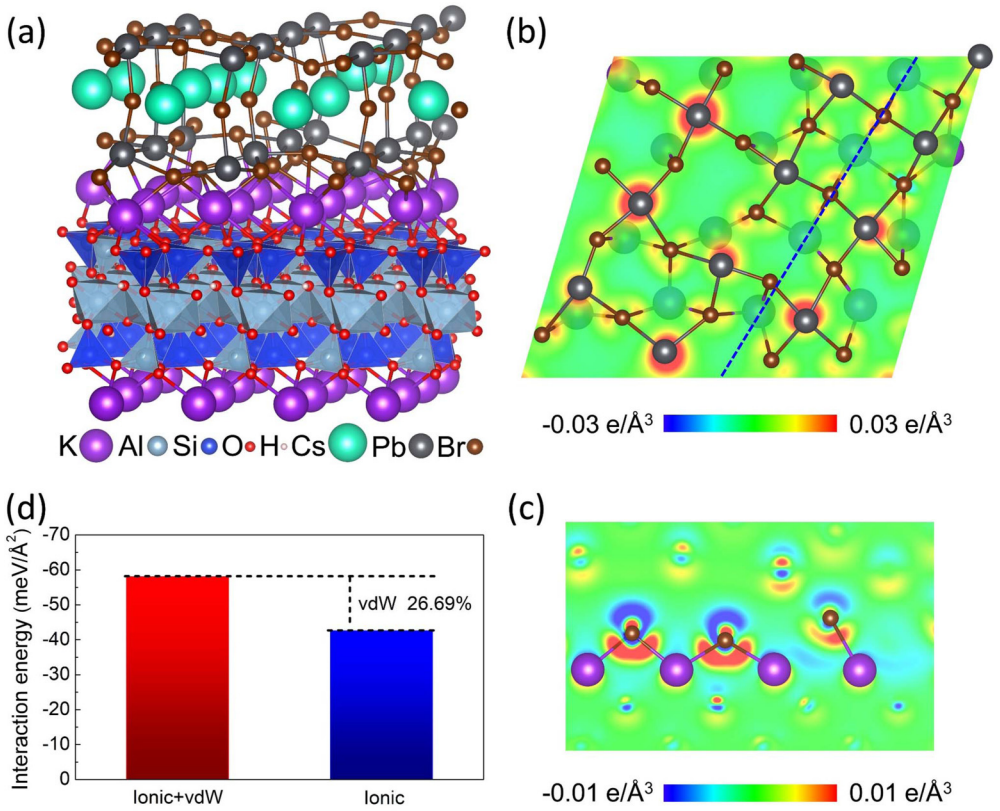

FIG. 4. DFT simulation of the interfacial interaction between the epitaxial halide perovskite $CsPbBr_3$ and the mica substrate. (a) Atomistic model of the relaxed supercell used in DFT calculations. The atoms have been labeled and drawn to their relative sizes. (b) The planar view of atomic stacking and charge transfer at the $CsPbBr_3$/mica interface. (c) Cross section noted as the blue dashed line in (b), and a significant charge transfer between the potassium and the bromine atoms can be observed. (d) Calculation of the interaction energy at the interface that with and without vdW interactions. The vdW interaction takes a significant portion of the overall interaction energy, meaning a relatively strong vdW force.

exchange-correlation functional [43,44] was used to describe the dispersion interaction (vdW forces) approximately as it has been demonstrated to be among the most accurate vdW functionals [45]. The plane-wave basis kinetic-energy cutoff was set to 400 eV. In the simulation supercell, the mica was selected as the substrate, and three layers of $CsPbBr_3$ lattices were covered on the mica surface to simulate the growth interface. The top K atom layers of mica and the three layers of the $CsPbBr_3$ lattices were allowed to relax until the forces on all the relaxed atoms were less than 0.05 eV/Å. The rotation angle between mica and $CsPbBr_3$ was selected as 33.69°, mainly by considering the following reasons: to decrease the macrostrain imposed on the $CsPbBr_3$ lattice and reduce the consumption of the computational resource.

Figure 4(a) is the relaxed mica/$CsPbBr_3$ supercell, and we can clearly observe the distortion at the interface of mica/$CsPbBr_3$. Due to the lattice/symmetry mismatch between mica and $CsPbBr_3$, an incommensurate interface is formed. Figure 4(b) shows the atomic stacking and charge-transfer distribution in the planar view between mica and $CsPbBr_3$, clearly illustrating the distortion at the interface. Figure 4(c) illustrates the cross section of the blue dashed line noted in Fig. 4(b) where the strong ionic interaction between the K layer of mica and the PbBr layer of $CsPbBr_3$ could be observed. The existing strain at the mica/$CsPbBr_3$ interface will consequently influence the $CsPbBr_3$ electronic band structure as well as the PL spectra, and the effects will attenuate with the $CsPbBr_3$ thickness increasing, which might be closely related with the thickness dependence of the blueshift of the PL peaks.

The characteristics of the interfacial interactions between mica and $CsPbBr_3$ is then determined by the contributions of the ionic and vdW interaction through comparing the difference between interaction energies of the nonlocal correlation functional and the one without it [13]. In the two calculations, we first calculated the interfacial characteristics including both the ionic and the nonlocal vdW interactions with the optB86b-vdW functional [shown as the red column in Fig. 4(d)]. Then, utilizing the same atomic structure we calculated the ionic interface properties of mica/$CsPbBr_3$ with only the plain PBE functional and obtained the blue column in Fig. 4(d). Comparing with the two columns, we could distinguish the energy scale of the vdW interaction. The obtained results shown in Fig. 4(d) indicate that the ionic interactions play a major role at the interface, which is reflected by the effective charge transfer [corresponding to Fig. 4(c)], whereas the rest of the contribution of the vdW interaction could still reach up to 26.69% (about 20 meV/Å^2). This value is already a considerable fraction of chemical bond and goes far beyond the conventional assumption that the vdW interaction is orders of magnitude lower than a typical chemical bond. For example,

the calculated vdW energy at the interface is about 1/4 of the silicon (111) free surface energy of 76.8 meV/Å^2 [46] and several times higher than the surface energy of graphene of ∼ 3 meV/Å^2 [47], a typical value for conventional vdW bonding.

To summarize, in this paper we performed a series of attempts to understand what a strong vdW interaction could look like in the soft perovskite system. By the observations of various possible strain relaxation mechanisms including the formation of cracks/holes, the lattice constant-dependent incommensurate rotational epitaxy and the thickness-dependent PL/reflectance, we show that, if the material is soft enough, vdW epitaxy can also result in a nontrivial substrate-film interaction. DFT calculations confirmed the vdW interaction in our case can contribute over one-fourth of the interfacial interaction between the soft crystal and the vdW substrate, suggesting a substantial part of the strain-related phenomena could stem from vdW force.

The authors would like to acknowledge support from the National Key Research and Development Program of China (Grant No. 2017YFB0702100), the National Natural Science Foundation of China (Grants No. 51705017 and No. U1706221), the U.S. National Science Foundation under Award No. 1635520, and a Rensselaer Presidential Fellowship. The authors declare no competing financial interests.

[1] H. Margenau, Van der Waals forces, Rev. Mod. Phys. **11**, 1 (1939).

[2] Y. Zhang, Y.-W. Tan, H. L. Stormer, and P. Kim, Experimental observation of the quantum Hall effect and Berry's phase in graphene, Nature (London) **438**, 201 (2005).

[3] K. S. Novoselov, A. K. Geim, S. Morozov, D. Jiang, M. Katsnelson, I. Grigorieva, S. Dubonos, and A. A. Firsov, Two-dimensional gas of massless Dirac fermions in graphene, Nature (London) **438**, 197 (2005).

[4] D. Pacile, J. Meyer, Ç. Girit, and A. Zettl, The Two-dimensional phase of boron nitride: Few-atomic-layer sheets and suspended membranes, Appl. Phys. Lett. **92**, 133107 (2008).

[5] G. Eda, H. Yamaguchi, D. Voiry, T. Fujita, M. Chen, and M. Chhowalla, Photoluminescence from chemically exfoliated MoS_2, Nano Lett. **11**, 5111 (2011).

[6] H. Li, J. Wu, Z. Yin, and H. Zhang, Preparation and applications of mechanically exfoliated single-layer and multilayer MoS_2 and WSe_2 nanosheets, Acc. Chem. Res. **47**, 1067 (2014).

[7] A. Koma, Van der Waals epitaxy—a new epitaxial growth method for a highly lattice-mismatched system, Thin Solid Films **216**, 72 (1992).

[8] M. I. B. Utama, Q. Zhang, J. Zhang, Y. Yuan, F. J. Belarre, J. Arbiol, and Q. Xiong, Recent developments and future directions in the growth of nanostructures by van der Waals epitaxy, Nanoscale **5**, 3570 (2013).

[9] Y. Wang, Y. Shi, G. Xin, J. Lian, and J. Shi, Two-dimensional van der Waals epitaxy kinetics in a three-dimensional perovskite halide, Cryst. Growth Des. **15**, 4741 (2015).

[10] J. Wu, C. Tan, Z. Tan, Y. Liu, J. Yin, W. Dang, M. Wang, and H. Peng, Controlled synthesis of high-mobility atomically thin bismuth oxyselenide crystals, Nano Lett. **17**, 3021 (2017).

[11] J. Wu, H. Yuan, M. Meng, C. Chen, Y. Sun, Z. Chen, W. Dang, C. Tan, Y. Liu, and J. Yin, High electron mobility and quantum oscillations in non-encapsulated ultrathin semiconducting Bi_2O_2Se, Nat. Nanotechnol. **12**, 530 (2017).

[12] C. H. Lui, L. Liu, K. F. Mak, G. W. Flynn, and T. F. Heinz, Ultraflat graphene, Nature (London) **462**, 339 (2009).

[13] A. Rudenko, F. Keil, M. Katsnelson, and A. Lichtenstein, Graphene adhesion on mica: Role of surface morphology, Phys. Rev. B **83**, 045409 (2011).

[14] C. Jin, J. Kim, J. Suh, Z. Shi, B. Chen, X. Fan, M. Kam, K. Watanabe, T. Taniguchi, and S. Tongay, Interlayer electron–phonon coupling in WSe_2/hBN heterostructures, Nat. Phys. **13**, 127 (2017).

[15] R. Viswanathan, J. Zasadzinski, and D. Schwartz, *Proceedings of the Annual Meeting-Electron Microscopy Society of America* (JSTOR, 1993), pp. 514–514.

[16] C. Woods, L. Britnell, A. Eckmann, R. Ma, J. Lu, H. Guo, X. Lin, G. Yu, Y. Cao, and R. Gorbachev, Commensurate-incommensurate transition in graphene on hexagonal boron nitride. Nat. Phys. **10**, 451 (2014).

[17] Y. Wang, Y.-Y. Sun, S. Zhang, T.-M. Lu, and J. Shi, Band gap engineering of a soft inorganic compound PbI_2 by incommensurate van der Waals epitaxy, Appl. Phys. Lett. **108**, 013105 (2016).

[18] G. H. Ahn, M. Amani, H. Rasool, D.-H. Lien, J. P. Mastandrea, J. W. Ager III, M. Dubey, D. C. Chrzan, A. M. Minor, and A. Javey, Strain-engineered growth of two-dimensional materials, Nat. Commun. **8**, 608 (2017).

[19] N.-G. Park, Perovskite solar cells: An emerging photovoltaic technology, Mater. Today **18**, 65 (2015).

[20] M. D. McGehee, Perovskite solar cells: Continuing to soar, Nature Mater. **13**, 845 (2014).

[21] Q. Chen, N. De Marco, Y. M. Yang, T.-B. Song, C.-C. Chen, H. Zhao, Z. Hong, H. Zhou, and Y. Yang, Under the spotlight: The organic–inorganic hybrid halide perovskite for optoelectronic applications, Nano Today **10**, 355 (2015).

[22] Y. Wang, X. Sun, R. Shivanna, Y. Yang, Z. Chen, Y. Guo, G.-C. Wang, E. Wertz, F. Deschler, and Z. Cai, Photon transport in one-dimensional incommensurately epitaxial $CsPbX_3$ arrays, Nano Lett. **16**, 7974 (2016).

[23] Y. Rakita, S. R. Cohen, N. K. Kedem, G. Hodes, and D. Cahen, Mechanical properties of $APbX_3$ (A = Cs or CH_3NH_3; X = I or Br) perovskite single crystals, MRS Commun. **5**, 623 (2015).

[24] See Supplemental Material at http://link.aps.org/supplemental/10.1103/PhysRevMaterials.2.076002 for more details on materials and methods, characterizations setups, AFM, and synchrotron diffractions.

[25] L. B. Freund and S. Suresh, *Thin Film Materials: Stress, Defect Formation and Surface Evolution* (Cambridge University Press, Cambridge, U.K., 2004).

[26] W. K. Liu and M. B. Santos, *Thin Films: Heteroepitaxial Systems* (World Scientific, Singapore, 1999), Vol. 15.

[27] A. Baskaran and P. Smereka, Mechanisms of Stranski-Krastanov Growth, J. Appl. Phys. **111**, 044321 (2012).

[28] I. Daruka and A.-L. Barabási, Dislocation-Free Island Formation in Heteroepitaxial Growth: A Study at Equilibrium, Phys. Rev. Lett. **79**, 3708 (1997).

[29] A. D. Novaco and J. P. McTague, Orientational Epitaxy—the Orientational Ordering of Incommensurate Structures, Phys. Rev. Lett. **38**, 1286 (1977).

[30] C. G. Shaw, S. Fain, Jr., and M. Chinn, Observation of Orientational Ordering of Incommensurate Argon Monolayers on Graphite, Phys. Rev. Lett. **41**, 955 (1978).

[31] J. Liu, Y. Xue, Z. Wang, Z.-Q. Xu, C. Zheng, B. Weber, J. Song, Y. Wang, Y. Lu, and Y. Zhang, Two-dimensional $CH_3NH_3PbI_3$ perovskite: Synthesis and optoelectronic application, ACS Nano **10**, 3536 (2016).

[32] D. Li, G. Wang, H.-C. Cheng, C.-Y. Chen, H. Wu, Y. Liu, Y. Huang, and X. Duan, Size-dependent phase transition in methylammonium lead iodide perovskite microplate crystals, Nat. Commun. **7**, 11330 (2016).

[33] E. Oksenberg, E. Sanders, R. Popovitz-Biro, L. Houben, and E. Joselevich, Surface-guided $CsPbBr_3$ perovskite nanowires on flat and faceted sapphire with size-dependent photoluminescence and fast photoconductive response, Nano Lett. **18**, 424 (2017).

[34] J. S. Manser and P. V. Kamat, Band filling with free charge carriers in organometal halide perovskites, Nat. Photonics **8**, 737 (2014).

[35] Y. Fang, H. Wei, Q. Dong, and J. Huang, Quantification of re-absorption and re-emission processes to determine photon recycling efficiency in perovskite single crystals, Nat. Commun. **8**, 14417 (2017).

[36] Y. Yamada, T. Yamada, L. Q. Phuong, N. Maruyama, H. Nishimura, A. Wakamiya, Y. Murata, and Y. Kanemitsu, Dynamic optical properties of $CH_3NH_3PbI_3$ single crystals as revealed by one-and two-photon excited photoluminescence measurements, J. Am. Chem. Soc. **137**, 10456 (2015).

[37] Y. Wang, Z. Chen, F. Deschler, X. Sun, T.-M. Lu, E. A. Wertz, J.-M. Hu, and J. Shi, Epitaxial halide perovskite lateral double heterostructure, ACS Nano **11**, 3355 (2017).

[38] Y. Yang, M. Yang, K. Zhu, J. C. Johnson, J. J. Berry, J. Van De Lagemaat, and M. C. Beard, Large polarization-dependent exciton optical Stark effect in lead iodide perovskites, Nat. Commun. **7**, 12613 (2016).

[39] T. J. Jacobsson, L. J. Schwan, M. Ottosson, A. Hagfeldt, and T. Edvinsson, Determination of thermal expansion coefficients and locating the temperature-induced phase transition in methylammonium lead perovskites using x-ray diffraction, Inorg. Chem. **54**, 10678 (2015).

[40] L. Goldstein and B. Post, Thermal expansion coefficients of ruby muscovite mica, J. Appl. Phys. **40**, 3056 (1969).

[41] G. Kresse and J. Furthmüller, Efficient iterative schemes for ab initio total-energy calculations using a plane-wave basis set, Phys. Rev. B **54**, 11169 (1996).

[42] P. E. Blöchl, Projector augmented-wave method, Phys. Rev. B **50**, 17953 (1994).

[43] J. Klimeš, D. R. Bowler, and A. Michaelides, Chemical accuracy for the van der Waals density functional, J. Phys.: Condens. Matter **22**, 022201 (2010).

[44] J. Klimeš, D. R. Bowler, and A. Michaelides, Van der Waals density functionals applied to solids, Phys. Rev. B **83**, 195131 (2011).

[45] T. Björkman, Testing several recent van der Waals density functionals for layered structures, J. Chem. Phys. **141**, 074708 (2014).

[46] B. E. Deal, The oxidation of silicon in dry oxygen, wet oxygen, and steam, J. Electrochem. Soc. **110**, 527 (1963).

[47] A. Kozbial, Z. Li, C. Conaway, R. McGinley, S. Dhingra, V. Vahdat, F. Zhou, B. D'Urso, H. Liu, and L. Li, Study on the surface energy of graphene by contact angle measurements, Langmuir **30**, 8598 (2014).